INTERNATIONAL JOURNAL FOR NUMERICAL METHODS IN FLUIDS, VOL. 22, 979–985 (1996)

A METHOD OF ASSESSING THE EFFECTS OF ARTIFICIAL DISSIPATION IN NAVIER–STOKES CODES

M. N. MACROSSAN AND M. HANCOCK

Department of Mechanical Engineering, University of Queensland, Brisbane 4072, Australia

SUMMARY

A new method of estimating the extent of the artificial dissipation effects in any solution obtained with a Navier–Stokes flow solver is described. Rather than recalculating the flow on a more refined grid, the solver may be used on the same grid to calculate the flow of an 'artificially dissipative fluid', which is a fluid having dissipate properties which arise entirely from the solution method itself. This is done by setting the viscosity and heat conduction coefficients in the Navier–Stokes solver to zero everywhere in the flow, while at the same time applying the usual boundary conditions at solid boundaries. An 'artificially dissipative flow' solution will be found where the dissipation effects depend entirely on the solver itself. By comparing this solution with that obtained on the same grid with the solver working in its normal mode, one can estimate whether further grid refinement is required, without necessarily producing an extensive series of solutions on different grids.

KEY WORDS: viscous flow; artificial dissipation; solution accuracy

1. INTRODUCTION

It is well known that numerical schemes for the solution of the governing equations of fluid mechanics can introduce errors which can be interpreted as arising from an artificial viscosity and heat conduction which are inherent in the solution method itself. Often the magnitude and nature of this inherent artificial dissipation cannot be quantified theoretically. It is the purpose of this work to present a method whereby the effect of the artificial viscosity and heat conduction can be readily estimated for a particular flow and a particular grid.

The method is to simulate a viscous, heat-conducting flow where the dissipative properties of the simulated fluid *arise entirely from the numerical method* itself. This is done by applying a standard Navier–Stokes computational method to a particular problem, but specifying that the physical viscosity and thermal conductivity of the fluid are zero everywhere throughout the flow. At solid wall boundaries the usual no-slip and thermally conducting surface conditions are applied and the stresses acting on the fluid in contact with the boundary are calculated using the correct physical viscosity and thermal conductivity for the problem under consideration.

Under these conditions a perfect numerical method would be set the apparently impossible task of finding a solution of the Euler equations for an ideal fluid with boundary conditions appropriate to a dissipative fluid; vorticity and energy would be injected into the flow by the wall boundary condition and, since there should be no way for these quantities to dissipate away from the wall in an ideal fluid, vorticity and energy should accumulate to infinite or non-physical values. An indication of a very good Navier–Stokes code might be that it fails in some catastrophic way under these conditions.

CCC 0271–2091/96/100979–07

Received November 1994
Revised August 1995

In practice, however, a solution may be obtained which contains the expected features of a dissipative flow. It is a wise precaution then to inspect the solution which is produced for the artificial fluid and compare it with the solution produced by the method working in its normal mode. For example, if the thickness of boundary layer developed for the artificial fluid is small compared with the boundary layer thickness developed by the solver working in its normal mode, this would be a strong indication that the artificial dissipation is negligible and the solver is reliable for that particular problem and that particular grid. If not, then further grid refinement is required.

Examples are given here of the boundary layers developed in a simple test flow for the artificially dissipative fluid associated with three Navier–Stokes solvers.

2. THE NAVIER–STOKES EQUATIONS IN FINITE VOLUME FORM

Consider a space (x, y, z) divided into N contiguous elements of volume V_j for $j = 1, \ldots, N$. Let S be the surface of V_j and $\hat{\mathbf{n}}$ the outward normal and let the unit vectors $\hat{\mathbf{p}}$ and $\hat{\mathbf{q}}$ form, with $\hat{\mathbf{n}}$, an orthogonal set of local axes at the surface S. Denote the components of the local fluid velocity $\mathbf{v}$ relative to these axes as (v_n, v_p, v_q). The Navier–Stokes equations can be written for each volume V_j as

$$\frac{\partial}{\partial t}\int_{V_j} \mathbf{U}\, \mathrm{d}V + \int_S (\mathbf{F}_\mathrm{E} + \mathbf{F}_\mathrm{D})\, \mathrm{d}S = 0, \tag{1}$$

where

$$\mathbf{U} = \begin{pmatrix} \rho \\ \rho v_n \\ \rho v_p \\ \rho v_q \\ \rho(\frac{1}{2}\mathbf{v}^2 + e_{\mathrm{int}}) \end{pmatrix} \tag{2}$$

For brevity in (2) we have not written the necessary transformation of momentum from a varying set of axes $(n - p - q)$ attached to a surface element of the control volume to a global fixed set of axes.

In (1) the fluxes across S are written in two parts: the *Euler* fluxes

$$\mathbf{F}_\mathrm{E} = \begin{pmatrix} \rho v_n \\ \rho v_n v_n + \rho RT \\ \rho v_n v_p \\ \rho v_n v_q \\ \rho v_n[\frac{1}{2}\mathbf{v}\cdot\mathbf{v} + \gamma RT/(\gamma - 1)] \end{pmatrix} \tag{3}$$

and the Navier–Stokes *dissipative* fluxes

$$\mathbf{F}_\mathrm{D} = \begin{pmatrix} 0 \\ -\tau_{nn} \\ -\tau_{np} \\ -\tau_{nq} \\ -(v_n\tau_{nn} + v_p\tau_{np} + v_q\tau_{nq}) + \phi_n \end{pmatrix} \tag{4}$$

In (2), e_{int} is the specific internal energy and a perfect gas equation of state, $p = \rho RT = \rho(\gamma - 1)e_{\mathrm{int}}$, where R is the ordinary gas constant, has been assumed.

The τ_{nj} in (4) are the stresses (excluding the thermodynamic pressure) acting on the surface S and ϕ_n is the component of the heat flux vector normal to S. These are related to the strains in the fluid by the constitutive relations

$$\tau_{nn} = (4\mu/3 + \mu_B)\partial v_n/\partial x_n + (\mu_B - 2\mu/3)(\partial v_p/\partial x_p + \partial v_q/\partial x_q), \tag{5}$$

$$\tau_{np} = \mu(\partial v_n/\partial x_p + \partial v_p/\partial x_n), \tag{6}$$

$$\tau_{nq} = \mu(\partial v_n/\partial x_q + \partial v_q/\partial x_n), \tag{7}$$

$$\phi_n = -\kappa\, \partial T/\partial x_n, \tag{8}$$

where μ, μ_B and κ are the coefficients of dynamic viscosity, bulk viscosity and thermal conductivity respectively and (x_n, x_p, x_q) are position co-ordinates measured in the directions of the unit vectors $\hat{\mathbf{n}}$, $\hat{\mathbf{p}}$ and $\hat{\mathbf{q}}$ attached to the surface S.

It is common to construct a Navier–Stokes solver by taking a Euler solver with its set of fluxes and adding in the appropriate Navier–Stokes dissipative fluxes. The Euler solver will make some estimate of the fluxes which could be written as $\mathbf{F}_E + \mathbf{F}_A$ to show that this estimate will contain some errors $\mathbf{F}_A$ which are the artificial dissipative terms. The magnitude of $\mathbf{F}_A$ may vary from point to point in the grid. When the Navier–Stokes (physically correct) dissipative terms are added, the final flux terms in the governing equations become $\mathbf{F}_E + \mathbf{F}_A + \mathbf{F}_D$ (where we have ignored any error in the estimation of $\mathbf{F}_D$). Clearly, for the Navier–Stokes solver to be accurate, we require that $|\mathbf{F}_A| \ll |\mathbf{F}_D|$.

3. TEST CASE: COMPRESSIBLE FLOW OVER A FLAT PLATE

The test case is one that has been used previously[1–3] to test some finite volume Navier–Stokes codes. The body is a flat plate aligned parallel to the freestream velocity. The freestream Mach number and temperature are $M_1 = 2$ and $T_1 = 222$ K and the wall temperature is fixed at $T_w = T_1$. A perfect gas with a ratio of specific heats of $\gamma = 1{\cdot}4$ is assumed and the viscosity of the gas is given by a Sutherland viscosity law

$$\mu = \mu_0(T/T_0)(T_0 + S_v)/(T + S_v), \tag{9}$$

where μ_0 and T_0 are reference quantities and $S_v = 110{\cdot}4$ K is a constant. The thermal conductivity is given by

$$k = C_p\, \mu/Pr, \tag{10}$$

where C_p is the specific heat at constant pressure and $Pr = 0{\cdot}72$ is the constant Prandtl number. The freestream Reynolds number based on the plate length L is $Re_L = 1{\cdot}65 \times 10^5$.

A spectral boundary layer solution, which was obtained by Jacobs[1] using the method of Pruett and Street,[4] is available for this case. The temperature profile across the boundary layer at the station $x/L = 0{\cdot}916$ is shown in Figure 1. There is a slight error in the boundary condition for the spectral solution, where freestream conditions have been imposed at the edge of the boundary layer. The finite volume solutions later contain the weak oblique leading edge interaction shock (which is generated by the displacement effect of the boundary layer), so the conditions at the edge of the boundary layer are slightly different from the freestream conditions.

4. THREE FINITE VOLUME METHODS

The three methods for calculating the inviscid fluxes which are considered here are

(i) Pullin's equilibrium flux method (EFM)[5] (a kinetic-theory-based method)

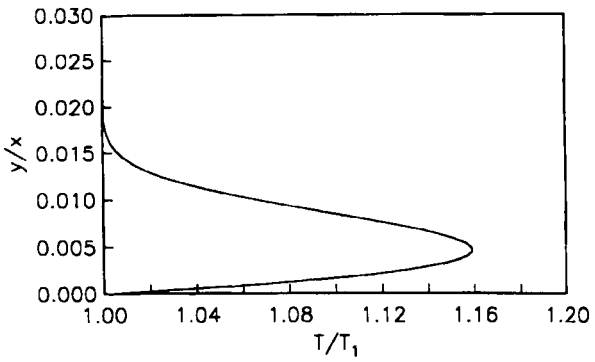

Figure 1. Spectral solution for temperature in boundary layer at $x/L = 0{\cdot}916$ $M_1 = 2{\cdot}0$, $Re_L = 1{\cdot}65 \times 10^5$, $T_1 = T_w = 222$ K

(ii) a Godunov scheme using an approximate Riemann solver[6]
(iii) the equilibrium interface method (EIM)[3] (a kinetic-theory-based Euler solver derived by eliminating most of the artificial dissipation from the equilibrium flux method).

A single code was used which had available the options of using any of these three methods to calculate the inviscid fluxes and also the option of invoking first- or second-order spatial accuracy when estimating the Euler fluxes. For first-order spatial accuracy, no gradients of any flow properties across the cells are assumed when estimating the states at cell interfaces; for second-order accuracy, linear (minmod) gradients of flow properties across cells are assumed. In both cases, second-order-accurate estimates of the gradients of flow properties necessary to determine the Navier–Stokes dissipative fluxes (see (5)–(8)) were calculated as described by Macrossan and Oliver[3].

Figure 2 shows the temperature variation through the boundary layer as calculated using the different methods, compared with the spectral solution. These results were obtained using the spatially *first-order* method and the same grid in each case. The smallest cell size in the y-direction was $\Delta y \approx 5 \times 10^{-4} L$ and there were approximately 25 cells across the boundary layer thickness. It can be seen that the EIM and Riemann solver give much better agreement with the spectral solution than does the EFM, which is clearly far more dissipative than the other methods. This is in accord with previous work which showed that while the EFM is robust and accurate for high-Mach-number flows, the artificial dissipation in the EFM increases for low Mach numbers.[2,7]

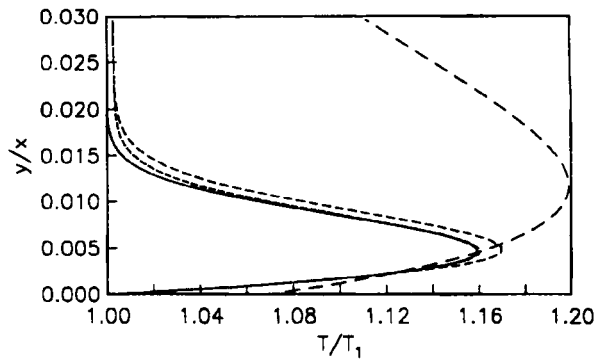

Figure 2. First-order finite volume methods compared with spectral solution (————) of Figure 1: – – – –, EIM; – – –, Riemann solver; – –, EFM (52 × 252 grid)

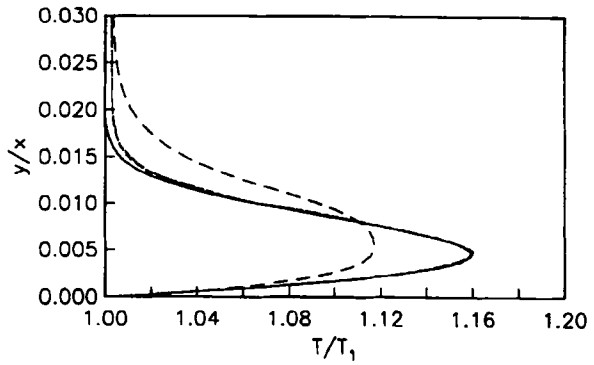

Figure 3. Second-order finite volume methods compared with spectral solution (————) of Figure 1: – – – –, EIM; – – –, Riemann solver; – –, EFM (52 × 252 grid)

An arbitrary measure of the boundary layer thickness Δ has been taken as the perpendicular distance to the surface from the point where the temperature ratio T/T_1 has fallen to 1·01. The boundary layer thicknesses so defined are: EIM, $\Delta/x = 15{\cdot}4 \times 10^{-3}$; Riemann, $\Delta/x = 16{\cdot}6 \times 10^{-3}$; EFM, $\Delta/x = 652{\cdot}9 \times 10^{-3}$. The results for the second-order versions of all these methods are shown in Figure 3. The boundary layer thicknesses for the second-order codes are: EIM, $\Delta/x = 15 \times 10^{-3}$; Riemann, $\Delta/x = 15 \times 10^{-3}$; EFM, $\Delta/x = 20{\cdot}8 \times 10^{-3}$. For later reference the 'exact' or 'true' boundary layer thickness has been taken as close to $\Delta_{ex}/x = 15 \times 10^{-3}$.

5. ARTIFICIALLY DISSIPATIVE FLOWS

To demonstrate the inherent artificial dissipation directly, we can show how a boundary layer develops when the no-slip, heat-conducting boundary condition is applied at the plate surface and when the flux terms everywhere else consist only of the solver's particular approximation to the Euler fluxes. The results for the second-order EFM are shown in Figure 4. The inherent dissipation induces a boundary layer of thickness $\Delta/x = 16{\cdot}7 \times 10^{-3}$, which is some 80% of the boundary layer thickness developed by the solver in its normal mode and is greater than the true boundary layer thickness. It is clear that the inherent dissipation in the second-order EFM on this grid is at least as great as the true Navier–Stokes dissipation.

Compared with the EFM, the other two methods have a small inherent artificial dissipation. Figure 5 shows the boundary layer developed from the inherent dissipation in the first- and second-order versions of the Riemann solver method. The temperature has fallen to below $1{\cdot}01T_w$ within seven cells from the surface for the first-order calculation and within five cells for the second-order calculation. The artificial boundary layer thickness Δ_a for the second-order calculation is $\Delta_a/x = 2{\cdot}33 \times 10^{-3}$. This is 15·5% of the boundary layer thickness predicted by the solver working in its normal mode and the results shown in Figure 3 indicate that the normal mode solution is very accurate. This suggests that the ratio Δ_a/Δ, which is the ratio of the artificial to normal mode boundary layer on the same grid, might be used to indicate whether any significant improvement in the solution would be obtained by repeating the calculation on a more refined grid.

Figure 6 shows a summary of results obtained for the three methods on a variety of different grids. Each data point shows, for a given numerical method and a given grid, the percentage deviation of Δ from the exact value as a function of the ratio Δ_a/Δ. As the ratio Δ_a/Δ falls below about 20%, the predicted boundary layer thickness is very accurate and little change is given by using a more refined

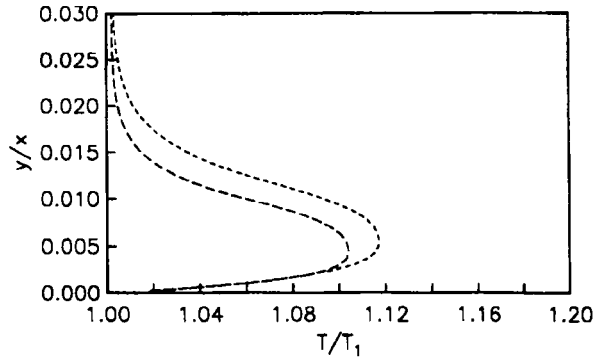

Figure 4. Second-order EFM results for no-slip and heat-conducting wall boundary condition with (– – –) and without (— — —) Navier–Stokes dissipative fluxes added in (52 × 252 grid)

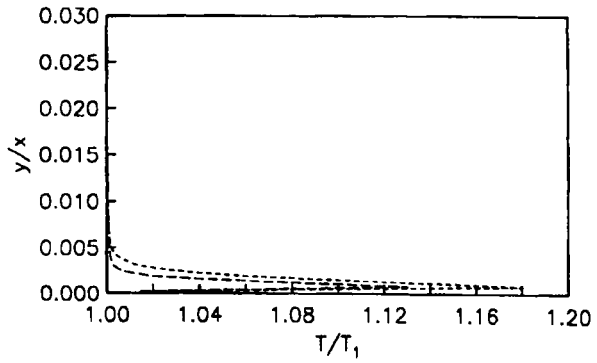

Figure 5. Inherent dissipation boundary layers for first- and second-order versions of Riemann solver method (52 × 252 grid)

grid. We propose that a value of $\Delta_a/\Delta < 18\%$ can be used as an indication that the grid is sufficiently refined and that no significant improvement would be obtained by repeating the calculation on a different grid. By this criterion the best solution shown in Figure 2 (first-order EIM), for which $\Delta_a/\Delta = 16{\cdot}7\%$, would be accepted and the others rejected, while both the EIM and Riemann solver solutions shown in Figure 3, for which $\Delta_a/\Delta = 12{\cdot}8\%$ and $15{\cdot}5\%$ respectively, would be accepted.

6. CONCLUSIONS

A method of estimating the effects of artificial dissipation in a solution method for the Navier–Stokes equations has been proposed. In this method a flow solution is developed in which the only dissipation is the artificial dissipation which is inherent in the method itself, except at the surface, where the usual Navier–Stokes boundary conditions are applied. A boundary layer develops, as a result of the inherent artificial dissipation of the method, and the thickness of this boundary layer compared with the thickness of the boundary layer predicted by the solver working in its normal mode illustrates how much the artificial dissipation can affect the solution. In other, more complicated flows, different dissipative effects will be apparent and we expect that these effects will also be produced in the artificially dissipative flow.

Before relying on any numerical solution of the Navier–Stokes equations obtained in any new application, it would be wise to compare that solution with what we have called the 'artificially

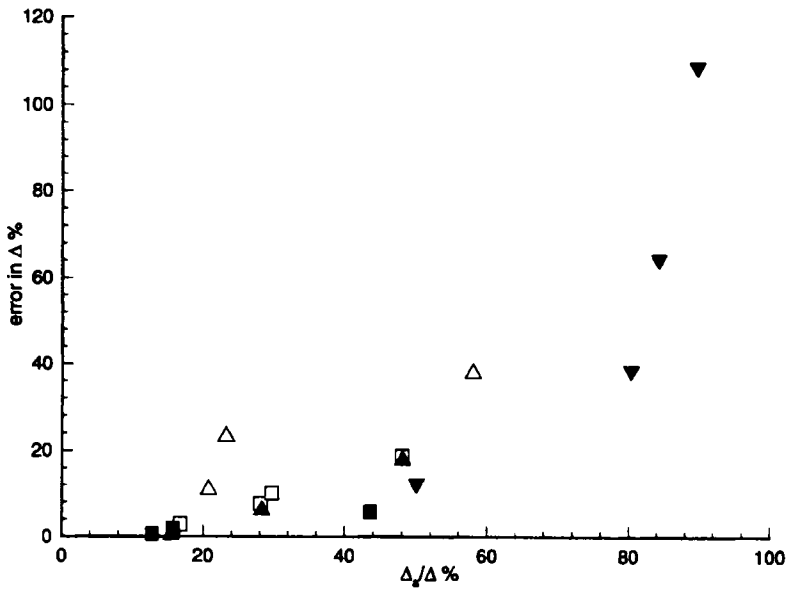

Figure 6. Error in predicted boundary layer thickness Δ for different numerical methods and grids: □, first-order EIM; ■, second-order EIM; △, first-order Riemann solver; ▲, second-order Riemann solver; ▼, second-order EFM (26 × 126, 52 × 63, 52 × 126, 52 × 252 and 52 × 504 grids)

dissipative solution' on the same grid. This is a much less computationally expensive task than that of repeating the calculation on a finer grid. It is suggested that if the artificially dissipative effects can be estimated to be less than about 18% of the dissipative effects seen when the solution method is working in its normal mode, then it is likely that there will be little point in repeating the calculation on a finer grid.

It is not likely that grid refinement studies or extrapolation techniques can be entirely abandoned in favour of the method proposed here, but an inspection of the artificially dissipative flow solution can provide a salutary insight concerning the artificial dissipation contained in a numerical solution of the Navier–Stokes equations. As experience is gained in assessing solution accuracy by this method, new criteria for what is an acceptably grid-independent numerical solution of the Navier–Stokes equations might be developed.

ACKNOWLEDGEMENT

This work was supported by the Australian Research Council under grant number A 89031403.

REFERENCES

1. P. A. Jacobs, 'Single-block Navier–Stokes integrator', *NASA CR-187613, ICASE Interim Rep. 18*, 1991.
2. E. R. Mallett, 'A numerical study of hypersonic leeward flow over the delta wing of the Hermes spacecraft using a parallel architecture supercomputer', *Ph.D. Thesis*, Department of Mechanical Engineering, University of Queensland, 1993.
3. M. N. Macrossan and R. I. Oliver, 'Kinetic theory solution methods for the Navier–Stokes equations', *Int. j. numer. methods fluids*, **17**, 177 (1993).
4. C. D. Pruett and C. L. Street, 'A spectral collocation method for compressible, nonsimilar boundary layers', *Int. j. numer. methods fluids*, **13**, 713 (1991).
5. D. I. Pullin, 'Direct simulation methods for compressible ideal-gas flow', *J. Comput. Phys.*, **34**, 231 (1980).
6. P. A. Jacobs, 'Approximate Riemann solver for hypervelocity flows', *AIAA J.*, **30**, 2555 (1992).
7. M. N. Macrossan, 'The equilibrium flux method for the calculation of flows with non-equilibrium chemical reactions', *J. Comput. Phys.*, **80**, 204 (1989).